Spatio-Temporal Evolution Monitoring and Analysis of Tidal Flats in Beibu Gulf From 1987 to 2021 Using Multisource Remote Sensing

Ertao Gao, Guoqing Zhou, *Senior Member, IEEE*, Shuxian Li, *Student Member, IEEE*, Bolin Fu, Yunzhi Xiao, Yanping Lan, Feng Wang, Jiasheng Xu, Qiang Zhu, and Yuhang Bai

***Abstract*—Tidal flats are an important part of coastal wetland systems and play an irreplaceable role in maintaining the health of global coastal ecosystems, resisting natural coastal disasters, and sequestering blue carbon. For the coastal zone around Beibu Gulf, where tidal flats are densely distributed, the spatiotemporal characteristics of tidal flats evolution and its key driving factors remain unclear. This article took the Beibu Gulf as the study area, and constructed an integrated tidal flats extraction algorithm of "maximum spectral index composite (MSIC) + Otsu algorithm (OTSU) + DEM correction" based on the cloud computing platform of Google Earth Engine to realize a large-scope and high-accuracy automatic extraction of tidal flats. The results discovered that 1) the tidal flats extraction method proposed in this study has high accuracy, with the overall accuracy of the confusion matrix reaching 93.9%, and the Kappa coefficient reaching 0.82. The user accuracy and mapping accuracy of the tidal flats are both greater than 85%. 2) In 35 years, the total tidal flats area of the Beibu Gulf has decreased by 683.9 km^2, a reduction of 29%, and the average annual rate of change was −19.5 km^2/a. 3) The fragmentation state of the tidal flats in Beibu Gulf intensified with time, and the natural driving forces of the tidal flats were mainly the rise in sea level, decrease in the amount of sediment in the river entering the sea, and expansion of mangrove trees. Human-driven forces were mainly coastal economic development and offshore aquaculture.**

Manuscript received 12 January 2024; revised 15 March 2024; accepted 1 May 2024. Date of publication 9 May 2024; date of current version 23 May 2024. This work was supported in part by the Guangxi Science and Technology Base and Talent Project under Grant # Guike AD19254002, and Grant AD23023012, in part by the Guangxi Natural Science Foundation under Grant 2023JJB150150, in part by the Guangxi University Young and Middle aged Teachers' Basic Scientific Research Ability Improvement Project under Grant 2023KY0265, in part by the Guangxi Natural Science Foundation for Innovation Research Team under Grant 2019GXNSFGA245001, in part by the National Natural Science Foundation of China under Grant 42371341, and in part by the BaGuiScholars program of Guangxi (Guoqing Zhou). *(Corresponding author: Guoqing Zhou.)*

Ertao Gao is with the College of Geomatics and Geoinformation, the Guangxi Key Laboratory of Spatial Information and Geomatics, the College of Earth Sciences, Guilin University of Technology, Guilin 541004, China.

Guoqing Zhou is with the Guangxi Key Laboratory of Spatial Information and Geomatics, the College of Earth Sciences, the College of Geomatics and Geoinformation and the College of Mechanical and Control Engineering, Guilin University of Technology, Guilin 541004, China, and also with the School of Microelectronics, Tianjin University, Tianjin 300072, China (e-mail: gzhou@glut.edu.cn).

Shuxian Li, Yunzhi Xiao, and Yanping Lan are with the College of Geomatics and Geoinformation, Guilin University of Technology, Guilin 541004, China.

Bolin Fu, Feng Wang, and Jiasheng Xu are with the College of Geomatics and Geoinformation, the Guangxi Key Laboratory of Spatial Information and Geomatics, Guilin University of Technology, Guilin 541004, China.

Qiang Zhu and Yuhang Bai are with the College of Earth Sciences, Guilin University of Technology, Guilin 541004, China.

Digital Object Identifier 10.1109/JSTARS.2024.3398604

***Index Terms*—Beibu gulf, drivers factor, spatio-temporal evolution, tidal flats, time series remote sensing.**

I. Introduction

TIDAL flats are located in the transition zone of the interaction between the sea and land, with dual characteristics of the sea and land [1], [2]. Tidal flats have rich natural resources and powerful ecosystems that play an important role in reducing the impacts of extreme storm surges, blue carbon sequestration, and the global greenhouse effect [3], [4]. More than 70% of the world's large- and medium-sized cities are located in coastal areas, accounting for more than 60% of the world's economy and 50% of the world's total population [5], [6], [7], [8], [9]. However, in recent years, with global warming, sea level rise, reduction of sediment transport in river basins, offshore aquaculture, reclamation, and construction of various coastal projects, the area of tidal flats has rapidly decreased, their natural properties are gradually weakening, biodiversity is decreasing, and their ability to resist typhoons and storm surges has weakened, threatening people's lives and property safety [10], [11], [12], [13], [14]. It has been estimated that the total tidal flat area decreased globally by more than 20000 km^2 between 1984 and 2016, representing a reduction of approximately 16% [15]. Therefore, the efficient and accurate acquisition of large-scale tidal flat resource distribution information, monitoring and analysis of the spatiotemporal evolution characteristics of tidal flats, and clarification of the main driving factors of the spatiotemporal evolution of tidal flats are important prerequisites for the protection of tidal flat resources, which have important practical significance and scientific value.

Early resource monitoring of tidal flats is typically based on field sampling surveys, relying mainly on traditional transport and equipment to conduct long-term surveys and sampling analyses of tidal wetlands [16]. However, poor accessibility, wide range, and rapid changes in tidal flats have resulted in samples from traditional field measurements not being able to fully reflect the real situation of tidal flats and not being able to carry out dynamic monitoring and analysis over long time series [17]. With improvements in the spectral, spatial, and temporal resolutions of remote sensing sensors, remote sensing technology is becoming increasingly suitable for extracting large-scale tidal flat information [18], [19]. LiDAR, UAVs, and

high-resolution satellite remote sensing imagery (WorldView, GeoEye-1, Beijing-3, etc.) can be used for high-precision tidal flat extraction at the regional scale; however, the data coverage is limited and expensive, and the performance of the application is low in the large-scale range [20], [21], [22]. Currently, the Landsat and Sentinel series of open-source and easily accessible satellite images are often used to acquire large-scale tidal flats [1], [2], [15], [23], [24], [25].

Extensive research has been conducted on tidal flat extraction using remote sensing technology. Traditional supervised and unsupervised classification methods are effective for obtaining coastal land cover information. However, they are time-consuming, laborious, and prone to misclassification, which makes them difficult to apply to large-scale tidal flat extraction [26], [27]. Machine learning algorithms have strong learning and computing abilities and can be applied to complex coastal feature classification by integrating multisource remote sensing data [28]. However, periodic tidal inundation is the biggest challenge restricting the extraction of tidal flats, and accurately acquiring remote sensing images of low- and high-tide levels is key to accurately obtaining the distribution of tidal flats. Based on the regional tide correction model, Murray et al. [29], [30] used part of Landsat satellite remote sensing images to determine the high and low tide boundary lines by manually selecting thresholds and the normalized difference water index (NDWI) and obtained tidal flat information along the Yellow Sea coast of China. Gao and Zhou [31] proposed a tidal flats extraction method based on "threshold segmentation + tide level correction" using Landsat series and Sentinel-2 imagery in combination with tidal hydrographic data. The spatiotemporal distribution of tidal flats in Guangxi, China, from 1987 to 2021 and the interfeedback relationship between the spatiotemporal evolution of tidal flats and mangroves were extracted. Sagar et al. [32] obtained the extent of tidal flats in Australia from 1987 to 2015 using Landsat systematic images combined with the median pixel composition of NDWI. However, owing to environmental differences in different regions and tidal hydrological differences, these methods are affected when extracting large-scale tidal flats and are time-consuming, labor-intensive, and inefficient. Based on multitemporal Sentinel-2 multispectral images, Dai et al. [33] constructed a coastal zone tidal flat extraction index to extract the distribution of tidal flats by analyzing the differences in the spectral reflectance characteristics of different features on high- and low-tide images and selecting the wavebands that can reflect the characteristics of tidal flats [33]. However, it is easy to misclassify tidal flats over a wide area, in different areas, and of different types.

In recent years, with the development and use of Google Earth Engine (GEE) high-performance cloud computing platforms, remote sensing cloud computing and analysis capabilities have greatly improved, effectively studying earth science-related issues [34], [35]. Murray et al. [1] determined the global spatial distribution of tidal flats from 1984 to 2016 by establishing a machine learning classifier using the GEE cloud platform, combining the Landsat series of temporal images, and disclosing a dataset for use by scholars around the world. However, many training samples can be time-consuming and misclassify many breeding ponds and inland mudflats as tidal flats. Wang et al. [2] constructed a decision tree classification model using the GEE platform. They trained a small number of datasets to extract and analyze the interannual variation range of tidal flats and coastal wetlands in China from 1986 to 2016. However, some adjacent water features, such as salt pans and breeding ponds, affect the classification accuracy. Yang et al. [36] used the mNDWI index image obtained from Sentinel-2 optical remote sensing images at high tide, and Sentinel-1 SAR images obtained at low tide to carry out map algebraic calculations and selected an appropriate threshold value to segment it to draw the tidal flat boundary of Fuqing City in southeast China. This method somewhat reduces the mixing of land and mudflats; however, the subjective acquisition of thresholds is uncertain and difficult for large-scale tidal flat extraction. Jia et al. [25] proposed the MSIC-OA method based on many Sentinel-2 images over a long time series compared multiple spectral indices for different land classes. They realized automatic mapping of the intertidal zone map of China using the spectral index composite method and the Otsu algorithm [37]. This method is a better solution to the effect of periodic tidal inundation on mudflat extraction; however, because Sentinel-2 imagery has only been used in recent years, it was impossible to analyze the spatiotemporal evolution of tidal flats over a long time series. Therefore, it is necessary to construct a stable and accurate method to extract the distribution of tidal flats over a large range and long time series and analyze the spatiotemporal evolution characteristics and main driving factors of tidal flats.

In summary, these methods are affected by tide-level data, sample training results, image acquisition moment, and other data when extracting large-scale tidal flat information. Owing to drastic environmental changes in the intertidal zone and the conversion of various ground feature coverage types, it is difficult to quickly and accurately obtain large-scale tidal flat distributions. Therefore, there is a need for a method that can quickly, accurately, stably, automatically, and reliably acquire large-scale multitemporal tidal flat distributions.

To optimize the tidal flat extraction method, identify the area and distribution of tidal flats in Beibu Gulf, and comprehensively analyze the spatiotemporal characteristics of tidal flats in Beibu Gulf as well as the main driving factors, this study will collaborate with multisource data to complete the monitoring and comprehensive analysis of tidal flat resources in Beibu Gulf. The main objectives of this study were as follows.

1) Based on the Google Earth Engine cloud computing platform, a fast, stable, and accurate automatic tidal flats extraction algorithm was constructed to realize large-scale and high-accuracy extraction of tidal flats resources in Beibu Gulf.
2) Quantify the area and spatiotemporal changes of tidal flats in Beibu Gulf, and analyzed the spatiotemporal characteristics of tidal flats in Beibu Gulf, with the support of spatiotemporal tidal flats distribution data and topographic data from 1987 to 2021.
3) Comprehensively utilizing multi-source data such as spatiotemporal evolution characteristics of tidal flats, tidal hydrography, sea level change, and statistical yearbooks,

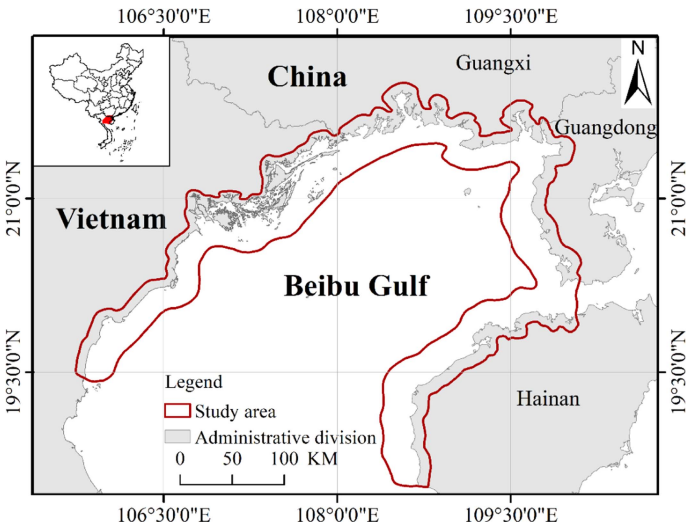

Fig. 1. Location of the study area.

to explore the key drivers of the spatiotemporal evolution of tidal flats in Beibu Gulf.

The results of this study provide references for the protection of tidal flats in Beibu Gulf and for the development of the coastal zone economy.

II. Materials

A. Study Area and Data Sources

This study considered the coastal zone around Beibu Gulf as the study area (see Fig. 1). Beibu Gulf, located in southwest mainland China, is a semi-enclosed bay surrounded by China and Vietnam. It reaches Guangxi Province, China, in the north, northern Vietnam in the west, Hainan Island, and the Leizhou Peninsula, China, in the east, and is connected to the Qiongzhou Strait and the South China Sea. The east-west width is approximately 110–180 nautical miles, with an area of approximately 128 000 km^2 [38]. Many rivers flow into Beibu Gulf, including Beilun River, Fangcheng River, Maoling River, Qinjiang River, Baiteng River, Red River, and Majiang River. Many rivers carry sediments and other materials from land to sea [39], which is an important material basis for the formation of tidal flats. Many tidal flats in Beibu Gulf include rock, gravel, mangroves, and muddy and sandy flats [31].

The experiment adopted the GEE cloud computing platform to obtain 4965 long-time series T1 Landsat surface reflectivity image data from 1987 to 2022 as the data source, as shown in Table I. The auxiliary DEM data were based on AW3D30 data with a spatial resolution of 30 m obtained from the Earth Observation Center of the Japanese Space Agency. Population, GDP, cargo throughput, and other data mainly came from the World Development Indicators released by the World Bank, the Resource and Environment Science and Data Center of China,[1] and the Transportation Department of Guangxi Province.[2]

[1][Online]. Available: https://www.resdc.cn/
[2][Online]. Available: http://jtt.gxzf.gov.cn/

TABLE I
Landsat Series Satellites Remote Sensing Images Information

Sensor type	Resolution (m)	Year	Number
Landsat5 TM	30	1987–2010	3132
Landsat5/7/8 ETM+/OLI	30	2011–2013	278
Landsat8 OLI	30	2014–2019	1042
Landsat9 OLI2	30	2020–2022	513

B. Data Preprocessing

This study used the cloud, shadow, and snow masking algorithm for cloud masking based on the QA quality assessment band. The quality and reliability of the image were improved by defining specific bit masks to label the pixels of clouds, shadows, and snow, which were then removed from the original image and analyzed in 12 observation periods over a 3-year time window. After cloud removal, the image stack obtained effective observation pixels and ensured the construction of a high-quality, dense time-sequence image stack for the study area. The maximum number of images covered by Landsat 5 imagery from 1987 to 2011 and Landsat 8 imagery from 2013 to 2021 were 737 and 503, respectively, and the corresponding percentages of effective observation pixels were 68.2% and 66.8%, respectively. The observable numbers of Landsat 7 images in 2012 and Landsat 9 images in 2022 are 15 and 33, respectively, and their effective observed pixels account for 75% and 82.5%, respectively. Image availability analysis can describe the coverage time range and frequency of image data and whether there are any missing data or discontinuities. It can evaluate the applicability and reliability of the image data.

III. Tidal Flats Extraction Method

Based on the support of a high-quality, dense time-sequence image stack, this study used NDWI and NDVI indices, and the maximum spectral index composite (MSIC) and Otsu algorithm were combined to achieve fast and automatic extraction of the tidal flat area in Beibu Gulf. The noisy pixels and misextracted information were removed using DEM data and a regional connectivity function, and the extent of tidal flats in the coastal zone of Beibu Gulf was accurately obtained. The key steps are as follows.

1) Calculation and comparison of spectral index: Two spectral indices, NDWI and MNDWI, were selected to calculate the geographical characteristics of the study area [40], [41]. Both have better sensitivity to water bodies and are more suitable for monitoring and extracting water bodies. The former typically combines green and near-infrared bands to distinguish between water and non-water bodies, whereas the latter uses green and mid-infrared bands. The spectral index calculation of the visualized images revealed that the NDWI index was less affected by the information of inland water bodies, such as breeding ponds, than the MNDWI index and had a certain shielding ability for the water bodies of breeding ponds. Although the

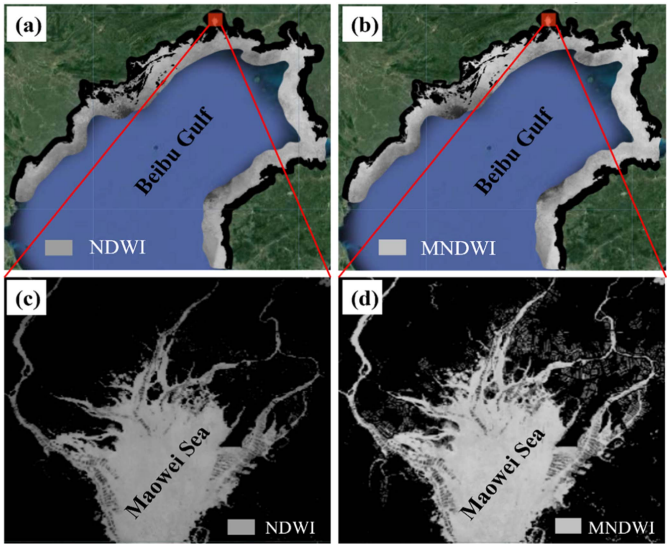

Fig. 2. Comparison of the results of different index calculations. (a) NDWI index. (b) MNDWI index. (c) NDWI Index of Maowei Sea in China. (d) MNDWI Index of Maowei Sea in China.

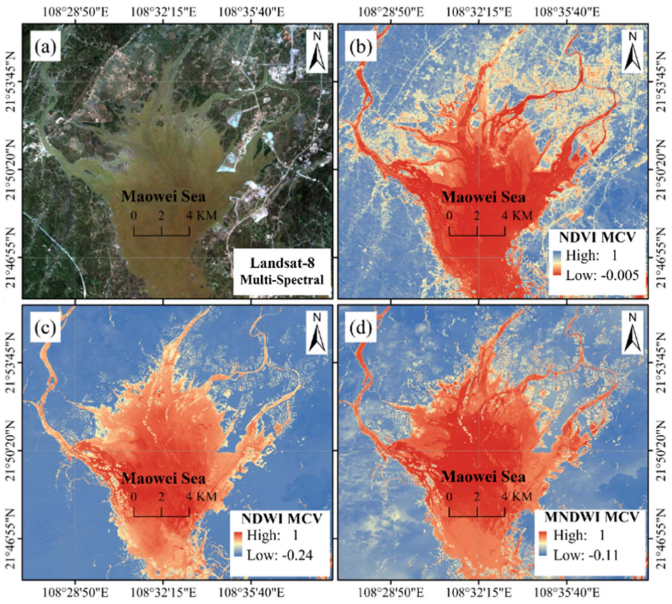

Fig. 3. MSIC synthesis results are based on a high-quality dense time sequence image stack. (a) True color synthesis. (b) NDVI maximum value synthesis. (c) NDWI maximum value synthesis. (d) MNDWI maximum value synthesis.

MNDWI value of water body pixels is significantly higher than that of NDWI, and the ability to enhance the water body information is relatively strong, most of the harbor areas in Beibu Gulf are dotted with numerous aquaculture ponds in the vicinity of the tidal flats. The information from these inland water bodies will seriously affect the effectiveness of tidal flat extraction. In addition, NDWI can effectively distinguish between vegetation and water bodies and, to a certain extent, avoid the misclassification of vegetation as water bodies. The results of the NDWI and MNDWI calculations are shown in Fig. 2.

2) Selection of high and low tide images using MSIC method: This study used the MSIC algorithm for maximum spectral index synthesis [42], [43], [44]. Synthetic images with high-quality pixel values were generated by selecting the maximum spectral value to synthesize each pixel in the image collection, thereby accurately acquiring the highest and lowest tide images during the observation period. Considering the Maowei Sea area in China as an example, the MSIC synthesis results during the observation period from 2017 to 2019 are shown in Fig. 3. We applied the MSIC algorithm to the Landsat high-quality dense time-series image stack for the observation periods in all target years. By selecting and analyzing the above spectral indices, it can be seen that NDWI can highlight the feature differences between water and nonwater pixels and simultaneously has a good inhibitory effect on vegetation and aquaculture pond water. Low-tide images obtained by NDVI can significantly enhance the feature differences among water bodies, tidal flats, and vegetation and, to some extent, avoid the interference caused by the uncertainty of tidal changes. Simultaneously, combined with the actual MSIC calculation results, the NDWI maximum composite value (MCV) and NDVI MCV images were used as the highest high-water and lowest low-water images in the observation period, respectively.

3) Threshold segmentation using the maximum interclass variance method (OTSU): Using the Otsu algorithm, the optimal segmentation threshold that maximizes the interclass variance and minimizes the intraclass variance is automatically selected to achieve binary segmentation of high- and low-tide images. The main processing steps were as follows:
   a) *Step1*: The highest and lowest tide images were first converted to grayscale images using NDWI and NDVI.
   b) *Step2*: The pixel statistics of the gray image were performed to obtain the number of pixels of each gray level, and the pixel probability of each gray level was calculated.
   c) *Step3*: The gray level was divided into two categories for each possible threshold: Those below the threshold as the background and those above or equal to the threshold as the foreground. The interclass variance under the current threshold was obtained, which was used to represent the degree of difference between the two categories. Then, find the threshold that minimizes the variance between classes as the optimal threshold value. The time series trends of NDWI and NDVI indices from 1987 to 2021 were shown in Fig. 4. In 2012, the automatically calculated threshold for the NDWI was 0.21, which stabilized in the range of 0.2 to 0.3 during the previous observation period. The threshold for the NDWI was significantly higher during the observation period of 2015–2018 than during the other years, whereas the trend of temporal variation in the NDVI was similar to that of the NDWI, with a stabilization threshold in the range of 0.31–0.37.

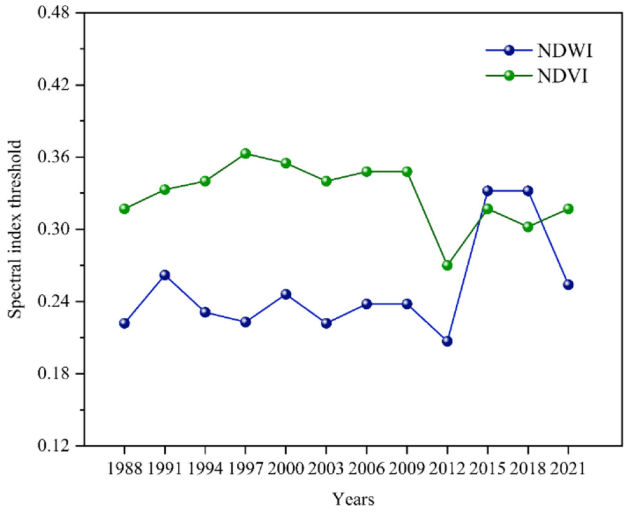

Fig. 4. Temporal changes of NDWI and NDVI from 1987 to 2021.

d) *Step4*: The maximum water surface result and the minimum water surface result were obtained automatically by binary segmentation of the highest water surface image and the lowest water surface image. Finally, the maximum and minimum water surfaces were superimposed on the mask to obtain the preliminary distribution information of the tidal flats. The results for the maximum and minimum water surfaces in the Maowei Sea are shown in Fig. 5.

4) Fine extraction of tidal flats using DEM data: To eliminate the false extraction of tidal flats caused by topographic relief, AW3D30 DEM data were used to calculate the tidal flat elevation. The results of the tidal flat extraction were spatially superimposed with the previous preliminary results, and the conditions of the results were filtered according to the set elevation threshold. Pixels or areas with elevation values below the threshold (which may represent inland water bodies) were masked or excluded while removing false extractions from high-elevation areas. Finally, the tidal flat extraction results after removing inland water bodies were observed through visualization and validation and further checked and adjusted to ensure the accuracy and reliability of the results. By programming and calculating the DEM elevation information, the maximum and minimum values of the DEM for the whole study area were obtained as 739 and −85 m, respectively, with an average of 7.8 m. The average slope of the study area was calculated to be approximately 0.08 using the DEM elevation and the width of the tidal flats. Since most of the inland ponds are manually excavated and have low topography, the elevation threshold was set to 0 m and the slope threshold was set to 0.08. These two thresholds were used to filter out tidal flats pixels with anomalous elevation and anomalous slopes, and minor adjustments were made to some areas in conjunction with visual interpretation. The results of removing the anomalous elevation pixels using the DEM are shown in Fig. 6.

TABLE II
OVERALL CONFUSION MATRIX OF TIDAL FLATS EXTRACTION FROM 1987 TO 2021

Category	Tidal flats	Non-tidal flats	Total	User accuracy
Tidal flats	1883	167	2050	92%
Non-tidal flats	384	4816	5200	93%
Total	2267	4983	7250	
Overall accuracy	92%		Kappa	0.82

The extraction results were smoothed to remove noise, eliminate isolated points, and minimize fluctuations to obtain a more continuous and accurate tidal flat boundary. Smoothing was performed using a majority filter based on morphological operations, which reduced noise and irregularities by considering the values of the pixels in the neighborhood and retaining multiple-valued pixels to smooth the extracted tidal flat results. Finally, the connectivity region to which each pixel belonged was calculated by analyzing the regional connectivity of the tidal flat pixels, calculating the number of pixels to which each pixel was connected, and assigning a unique region identifier to each pixel [45]. According to the test comparison, the eight-neighborhood connection method was selected in this study, which can effectively remove noise and fine mis extraction in the tidal flat extraction results to accurately extract tidal flat distribution. A comparison before and after false pixel shielding is shown in Fig. 7.

Based on the above method and process, this study obtained the distribution of tidal flats around Beibu Gulf from 1987 to 2021, and the overall technical process is shown in Fig. 8.

IV. RESULTS

A. Tidal Flats Extraction Accuracy Analysis

To test the accuracy of the experimental extraction results, we analyzed the tidal flat extraction results both quantitatively and qualitatively. The quantitative analysis combined with Sentinel-2 multispectral image data and randomly generated sample points to verify the accuracy of the extracted results [25]. In total, 7250 sample points were generated in this study, including 2050 tidal flats sample points and 5200 other sample points. The tidal flat and nontidal flat information was distinguished by human–computer interaction decoding, and the accuracy of the tidal flat range was evaluated by combining the confusion matrix method for all observation periods to obtain the overall confusion matrix of tidal flats extracted from 1987 to 2021 (see Table II). The overall accuracy and kappa coefficient reached 92% and 0.82, respectively, indicating that the accuracy of the tidal flat range extracted using the proposed method is relatively reliable.

In addition, this study also compared the accuracy of the tidal flats extraction results from the 1986 to 2016 global tidal

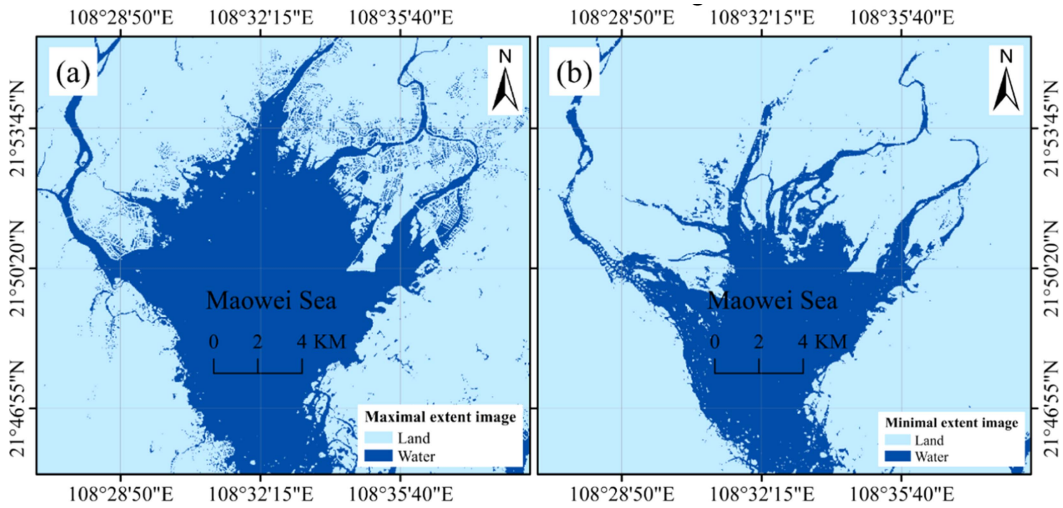

Fig. 5. Tidal flats boundary after binarization. (a) Maximum water surface results after threshold segmentation. (b) Minimum water surface results after threshold segmentation.

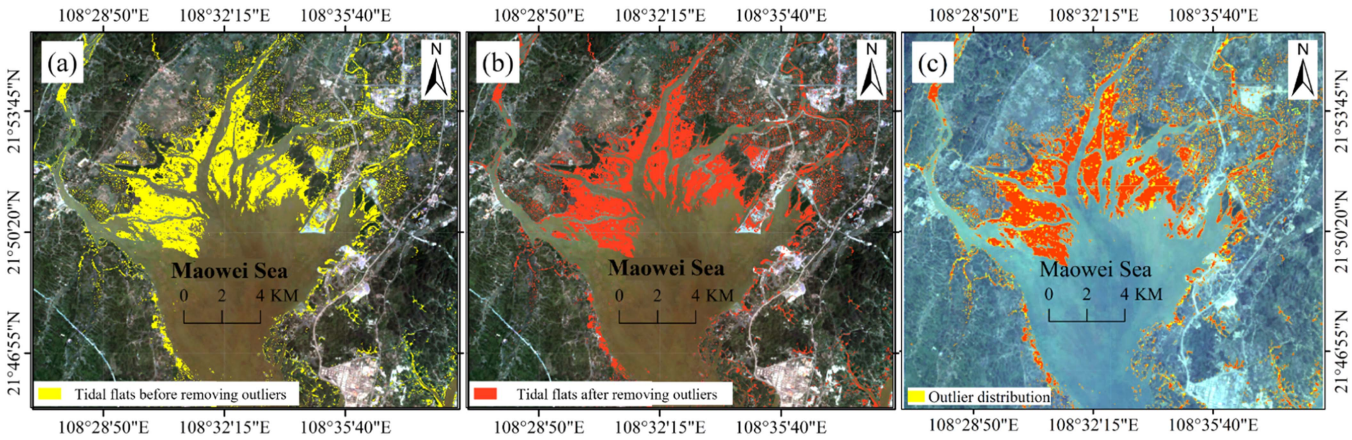

Fig. 6. Results of before and after removing outliers from tidal flats using DEM. (a) Before removing outliers; (b) After removing outliers. (c) Distribution of outliers.

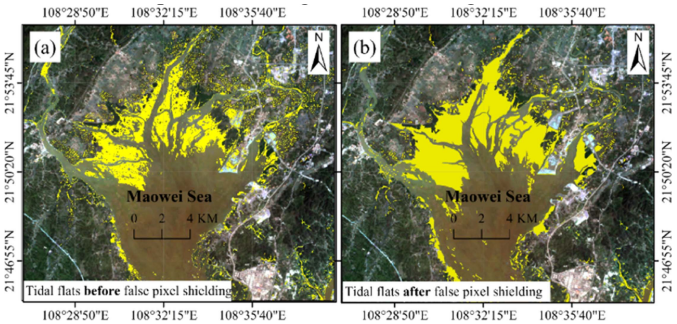

Fig. 7. Processing results based on pixel connectivity analysis. (a) False pixel shielding before. (b) False pixel shielding after.

flats dataset UQD (University of Queensland global tidal flat dataset) produced by Murray et al. [15] to analyze the tidal flats extraction results of each coastal segment of the Beibu Gulf. A comparison between the extracted tidal flat range and the UQD data in the Beihai and Qinzhou coastal of China showed that the UQD was consistent with the extracted range in this study (see Figs. 9 and Fig. 10). However, the small trench was slightly different, and parts of the inland fishponds in the UQD diagram were mistakenly divided into tidal flats [see Fig. 9(c) and (d)]. As shown in Fig. 10, UQD mistakenly identified some residential areas [see Fig. 10(d)] and inland lakeshores [the blue oval in Fig. 10(b)] as tidal flats in the coastal section of Qinzhou, China. The tidal flat extraction method proposed in this study can effectively extract the tidal flat distribution in coastal wetlands.

In conclusion, the integrated tidal flats extraction algorithm of "MSIC + OTSU + DEM correction" constructed in this study was able to obtain the distribution of large-scale tidal flats well, and the accuracy of the results was reliable. This method can be used to extract large-scale tidal flats long-distance coastlines, and classify coastal wetlands.

B. Characteristics of the General Changes of Tidal Flats in Beibu Gulf

The total area of tidal flats in Beibu Gulf and the time series changes of tidal flats in each coast section from 1987 to 2021

TABLE III
TIME-SERIES VARIATION OF TIDAL FLATS AREA ALONG THE BEIBU GULF (KM^2)

Year	The tidal flats of Vietnam coast section, Vietnam	The tidal flats from Guangxi to Guangdong coast section, China	The tidal flats from Guangdong to Hainan coast section, China	Total area of tidal flats in Beibu Gulf
1987	1208.8	866.8	280.0	2355.6
1991	993.9	733.3	224.2	1951.4
1994	991.0	706.6	218.5	1916.2
1997	1038.6	753.5	230.2	2022.3
2000	832.7	667.1	246.0	1745.7
2003	911.9	736.6	251.7	1900.1
2006	751.8	655.0	281.8	1688.6
2009	768.8	570.3	219.8	1559.0
2012	930.1	550.1	229.0	1709.2
2015	922.3	647.1	248.1	1811.5
2018	977.1	663.5	200.9	1841.5
2021	879.4	568.8	223.6	1671.7

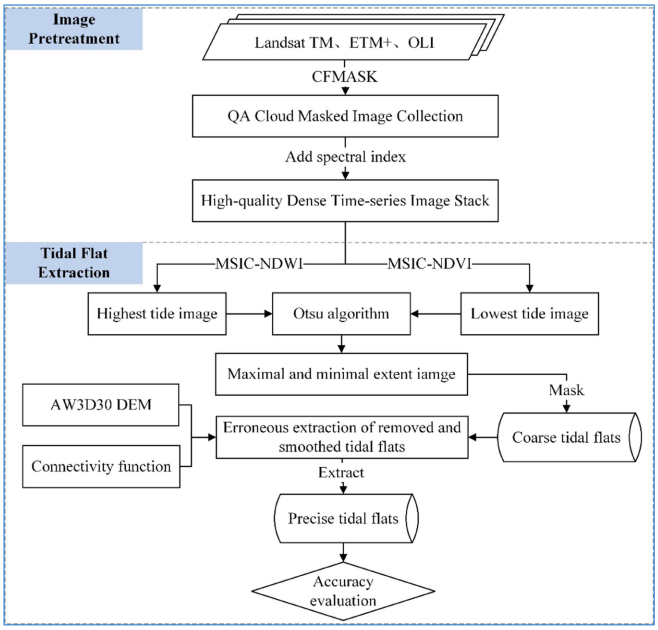

Fig. 8. Process of tidal flats extraction based on "MSIC + OTSU+ DEM correction".

are shown in Fig. 11 and Table III. In the past 35 years, the total tidal flats area of the Beibu Gulf has shown a decreasing trend, from 2355.6 km^2 in 1987 to 1671.7 km^2 in 2021, a total decrease of 683.9 km^2, with a reduction rate of 29.0%, and an average annual change rate of -19.5 km^2/a. As can be seen from Table III, the total tidal flat area of Beibu Gulf has shown an overall decreasing trend over the past 35 years. The area of the tidal flats greatly reduced from 1987 to 1991, with an area reduction of 404.2 km^2 and a reduction rate of -101.05 km^2/a. The tidal flats changed slightly from 1991 to 2003, and the overall tidal flat area changed very slowly from 1991 to 1994, remaining at approximately 1900 km^2. In 1997, the tidal flat area reached 2022.3 km^2, which increased slightly compared to 1916.2 km^2 in 1994. The tidal flat area significantly decreased between 1997 and 2000. In 2000, the tidal flat area was only 1745.7 km^2, a decrease of 13.7%. The period from 2000 to 2003 was the period of the largest increase in tidal flats area, with an increase of 8.8%. From 2003 to 2018, the total tidal flat area in the study area showed a continuous decreasing trend during the first three observation periods. By 2009, the tidal flat area had decreased to a minimum of 1559.0 km^2, and the total area of continuous reduction was 341.1 km^2, with a reduction rate of -56.85 km^2/a. However, it continued to increase in the last three observation periods, with an increase of 282.5 km^2 and an increase rate of 31.39 km^2/a. After 2018, the reduction in the tidal flat area was more evident, with a decrease of 9.2%.

C. Characteristics of Tidal Flat Area Changes in the Three Coastal Sections of Beibu Gulf

The coastline of the Beibu Gulf region is long and has a large longitudinal span. The distribution of tidal flats along the entire Beibu Gulf coast is uneven because of the distribution of estuaries, circulation, and other natural conditions. In this study, the coastal zone around Beibu Gulf was divided into three coastal sections for analysis: the coastal section of Vietnam (from the vicinity of Qinghua Cen Mountain in Vietnam to the mouth of the Beilun River in Vietnam), the coastal section from Guangxi to Guangdong, China (from the mouth of the Beilun River in China to the north of Zhanjiang Port in Guangdong Province of China), and the coastal section from Guangdong to Hainan of China (from Lemin Port in China to Yingge Bay in Hainan Province of China). Temporal changes in the tidal flat areas of the three coastal sections and their trends are shown in Fig. 12.

The tidal distribution characteristics of Vietnam are complex, with Quang Ninh City in the north and Hai Phong City in the center showing regular full-day, irregular half-day, and full-day parting tides, respectively [46]. The tidal flats formed over the

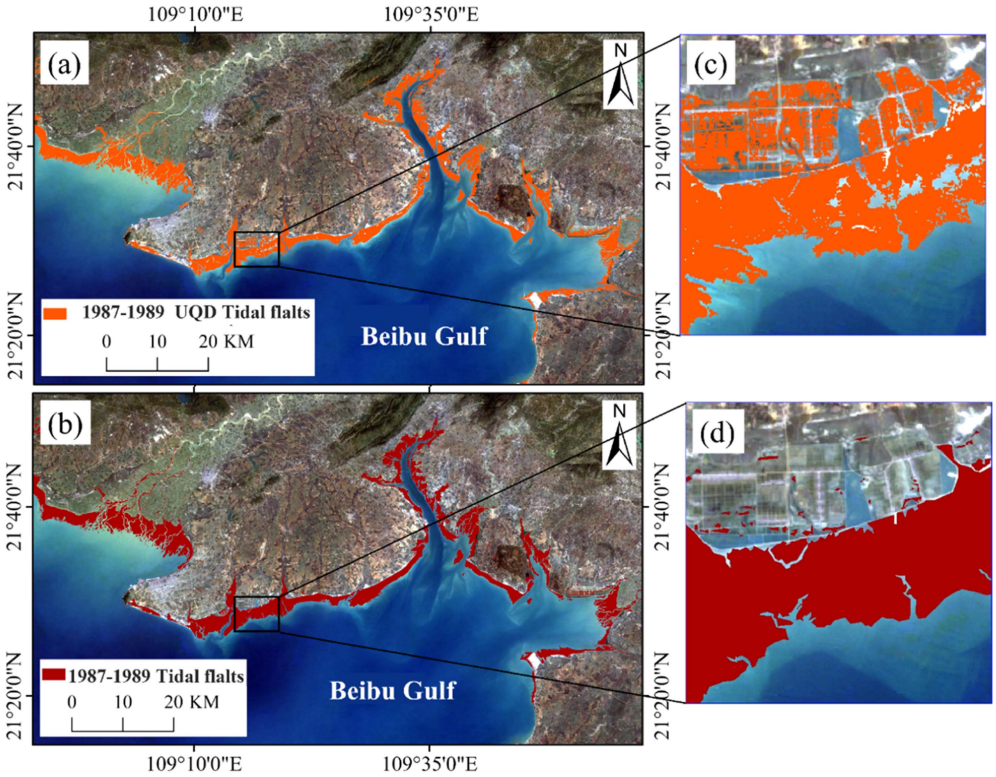

Fig. 9. Comparison of tidal flats extraction results with UQD in Beihai, China. (a) UQD tidal flats; (b) The tidal flats obtained in this study; (c) UQD incorrectly identifies fish ponds as tidal flats; (d) This study outperforms UQD in extraction details of tidal flats.

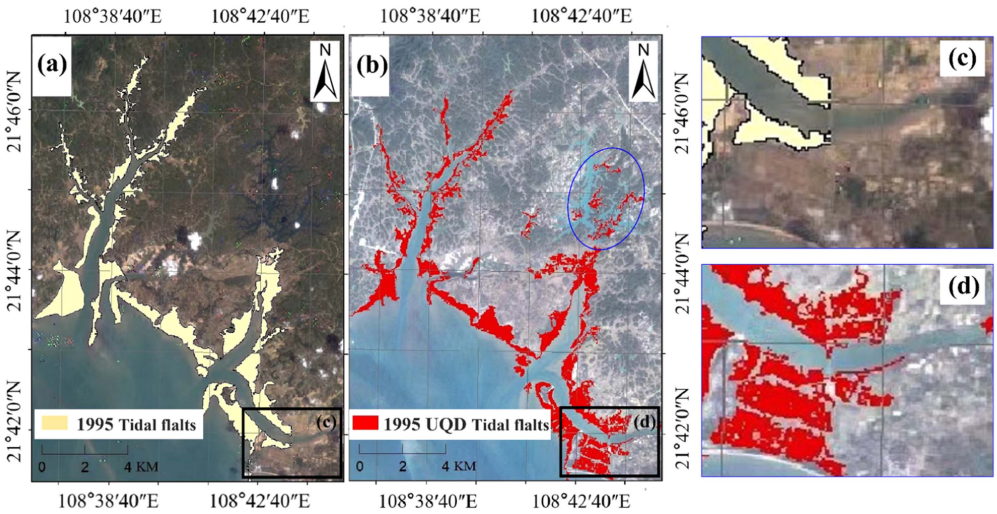

Fig. 10. Comparison of tidal flats extraction results with UQD in Qinzhou, China. (a) Tidal flats obtained in this study. (b) UQD tidal flats. (c) UQD incorrectly identifies part of the residential areas as tidal flats. (d) Details of tidal flats obtained in this study.

entire coastal section were mainly mangrove and sandy, muddy tidal flats, mainly concentrated near Quang Ninh City and Hai Phong City ports. As shown in Fig. 12, the coastal tidal flats of Vietnam are the largest part of the Beibu Gulf study area, with a maximum tidal flat area of 1208.8 km^2, accounting for 51.3% of the total tidal flat area of Beibu Gulf at the same time. The minimum tidal flat area was 751.8 km^2 in 2006, accounting for 44.5% of the total area during the same period. From 1987 to 2021, the total area of tidal flats decreased by 329.5 km^2, or 27.2%, with an average annual rate of change of -9.4 km^2/a. The decrease in tidal flats by 215 km^2 from 1987 to 1991 was similar to the overall change in the area of Beibu Gulf, which was the most obvious period of reduction; the change in tidal flats from 1991 to 1994 was very small, followed by an increase in 1997. The change in the tidal flat area between 1991 and 1994 was very small and then increased until 1997. From 2000 to 2012, the tidal flat area first increased, then decreased, and then increased slowly. The tidal flat area in 2006 was 751.8 km^2,

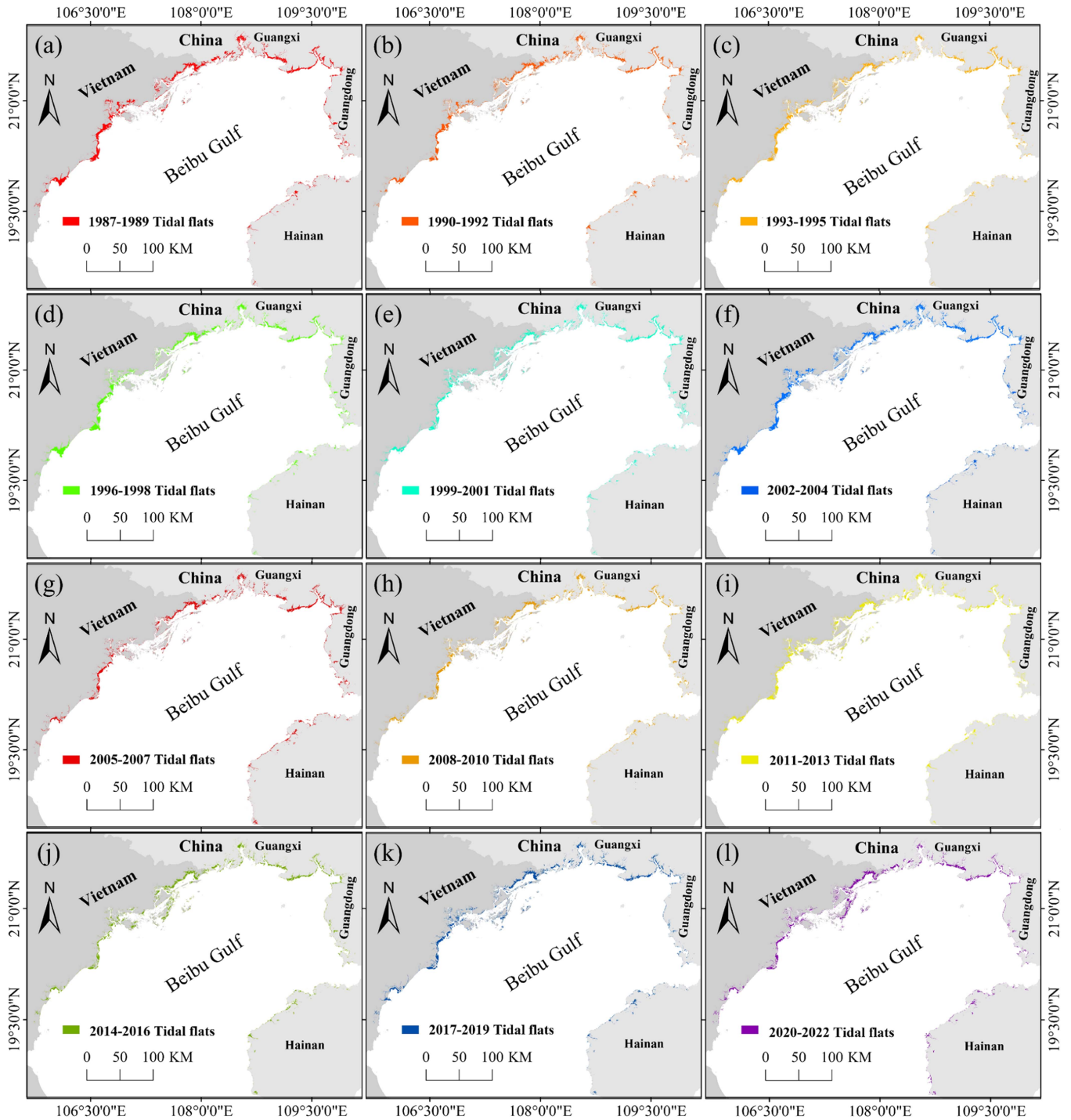

Fig. 11. Distribution of tidal flats in the Beibu Gulf from 1987 to 2021. (a) Distribution of tidal flats from 1987 to 1989. (b) Distribution of tidal flats from 1990 to 1992. (c) Distribution of tidal flats from 1993 to 1995. (d) Distribution of tidal flats from 1996 to 1998. (e) Distribution of tidal flats from 1999 to 2021. (f) Distribution of tidal flats from 2002 to 2004. (g) Distribution of tidal flats from 2005 to 20007. (h) Distribution of tidal flats from 2008 to 2010. (i) Distribution of tidal flats from 2011 to 2013. (j) Distribution of tidal flats from 2014 to 2016. (k) Distribution of tidal flats from 2017 to 2019. (l) Distribution of tidal flats from 2020 to 2022.

which was the period with the smallest change of the entire time series. The largest increase in tidal flats from 2009 to 2012 was 20.98%, with tidal flats reaching 930.1 km^2 by 2012. However, the overall tidal flat area did not change significantly from 2000 to 2012, with an increase of only 11.7%. In 2018, the tidal flat area rebounded, and increased to 977.1 km^2, close to the tidal flat area in 1994. From 2018 to 2021, the tidal flat area decreased significantly, with an area reduction of 97.7 km^2.

The tidal flats along the coast from Guangxi to Guangdong in China are more evenly distributed along the coasts of the three cities of Guangxi (Fangchenggang City, Qinzhou City, and Beihai City). They are most evident in seaport areas such as Pearl

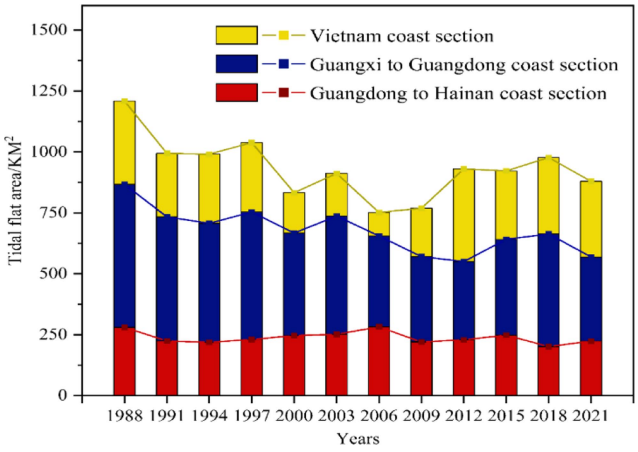

Fig. 12. Tidal flats area and trend of change in the three coast sections of Beibu Gulf.

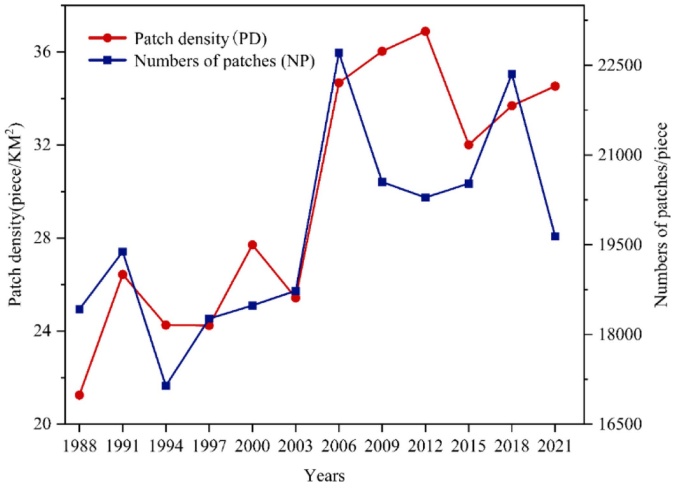

Fig. 13. Temporal variation of tidal flats landscape fragmentation from Guangxi to Guangdong in Beibu Gulf.

Harbor, Maowei Sea, and Beihai Harbor. From 1987 to 2021, the area of the tidal flats in this section decreased from 866.8 to 568.8 km^2, a total decrease of 298 km^2, or 34.4%, with an average annual rate of change of -8.5 km^2/a. From 1987 to 1994, the area of tidal flats decreased, reducing 160.2 km^2, or 18.5%. Among them, the period 1987 to 1991 was similar to that of the tidal flats along Vietnam and the entire tidal flats of Beibu Gulf. It was the period with the largest reduction of tidal flats, with an area reduction of 133.5 km^2, and an average annual rate of change of -33.4 km^2/a. The tidal flats showed a short continuum of slow growth from 1994 to 1997 and 2000 to 2003, with growth of 46.9 and 69.5 km^2 and growth rates of 15.6 and 23.2 km^2/a, respectively. The tidal flat area decreased during the four target years from 2003 to 2012. In 2012, the tidal flats area reached the minimum of 550.1 km^2, the area decreased by 186.5 km^2, the decrease amplitude reached 25.3%, and the change rate was -20.7 km^2/a. During the observation period from 2012 to 2018, the tidal flat area first increased to 663.5 km^2 in 2018, with an increase rate of 20.6% and a growth rate of 18.9 km^2/a. After 2018, the tidal flat area decreased significantly, and by 2021, the tidal flat stock is only 568.8 km^2.

The tidal flats from Guangdong to Hainan, China, are in Liusha Harbor in Guangdong, Yizhou Bay, and Yingchao Harbor in Hainan. From Fig. 12, it can be intuitively found that the distribution of tidal flats in the coastal section from Guangdong to Hainan was relatively scattered. Compared with the other two tidal flats, the area of the tidal flats in this section was smaller. Still, the temporal variation in the area was the most stable among the three sections, and the overall area of the tidal flats was maintained in the range of 200 to 280 km^2. From 1987 to 2021, the tidal flats area was reduced from 280 to 223.6 km^2, with a decrease of 56.4 km^2 and a decrease of 20.1%, and the annual rate of change is only -1.6 km^2/a. The largest tidal flat area was 281.8 km^2 in 2006, accounting for 16.7% of the total tidal flat area of Beibu Gulf during the same period, and the smallest area was 200.9 km^2 in 2018, accounting for only 10.9% of the area. Tidal flats were significantly reduced from 1987 to 1991, with 55.8 km^2 and 20% reduction, respectively. From 1991 to 1994, with a reduction of 5.7 km^2, a decrease of only 2.5%. The tidal flats showed a continuous slow growth trend over the next five target years, reaching a peak in 2006 with an increase of 63.3 km^2, but with a very low average annual rate of change of only 4.2 km^2/a. The tidal flats showed the greatest reduction of 22% from 2006 to 2009, with a -20.6 km^2/reduction rate. During the three observation periods from 2009 to 2015, the tidal flat area increased slightly, with an area growth of 28.3 km^2. The area changes of the tidal flats from 2015 to 2021 are contrary to those of the other two coast sections, showing a trend of first decreasing and then increasing. The area reduction and increase were 47.2 and 22.7 km^2, with reductions and increases of 19% and 11.3%.

V. Discussion

A. Characteristics of Tidal Flats Fragmentation

From the above analysis, it can be seen that the reduction in tidal flats from the Guangxi to Guangdong section between 1987 and 2021 was the largest among the three sections, reaching 34.4%, which was more than the average shrinkage of 29% in Beibu Gulf. This study analyzed the main drivers of the spatiotemporal evolution of tidal flats in detail using the section from Guangxi to Guangdong as an example. First, the fragmentation characteristics of the tidal flats from Guangxi to the Guangdong coast of Beibu Gulf were analyzed. The patch density (PD) fluctuated significantly, from 21.25 in 1987 to 36.88 in 2012, and the overall patch density showed a fluctuating upward trend (see Fig. 13). The change in the period from 1994 to 1997 was stable. From 2003 to 2006, fragmentation was extremely drastic, with an increase of 36.36% in the PD value, and the number of patches (NP) reached a maximum of 22 711 in 2006. After 2012, the PD value decreased sharply and then continued to increase. In 2015, it dropped to 32.01; the increase from 2015 to 2021 is 7.9%, and fragmentation continues to accelerate. By 2021, the number of tidal flat patches will be 19639, with a PD value of 34.53. The intensification of the fragmentation of the tidal flats indicates that they gradually increased under the influence of natural or human factors [47].

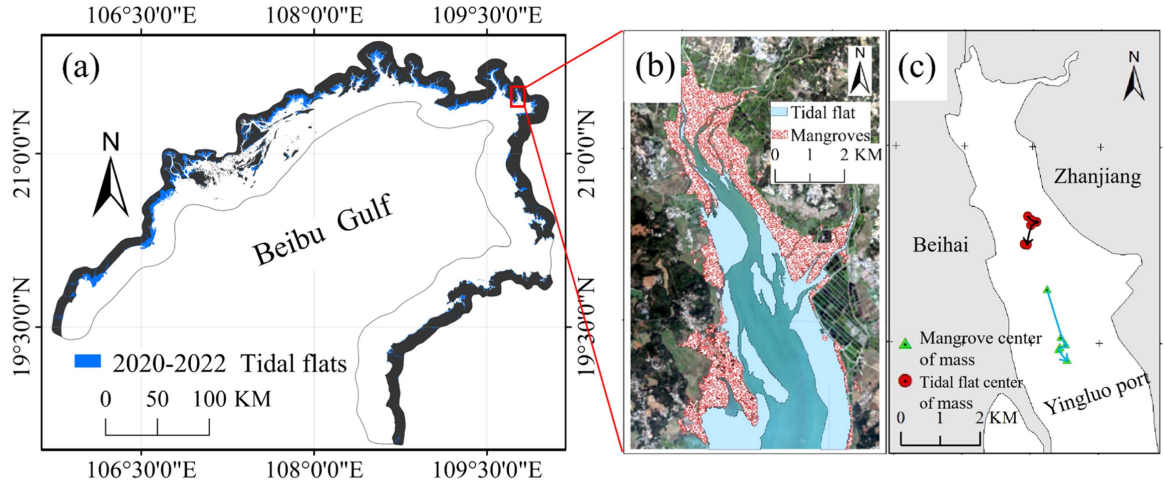

Fig. 14. Relationship between spatio-temporal distribution of tidal flats and mangrove forests in Shankou Mangrove National Reserve. (a) Location of Shankou Mangrove National Reserve. (b) Spatial distribution of mangroves and tidal flats in 2021. (c) Centroid transfer between mangroves and tidal flats.

B. Analysis of the Main Drivers of the Spatiotemporal Evolution of Tidal Flats in Beibu Gulf

1) Impacts of Sea Level Rise: Polar glaciers melt as the global climate continues to warm, causing the sea level to rise annually [10]. Sea level rise causes the mean shoreline (mean high and low tide lines) to move toward the land, resulting in a slower rate of tidal flat siltation and increased coastal erosion [48]. This study collected sea-level change data for Beibu Gulf from the China Sea Level Bulletin, published by the Ministry of Natural Resources of China.[3] According to statistics [49], since 1980, the coastal sea level of Beibu Gulf has shown a slow rising trend, and the rate of sea level rise from 1980 to 2019 was 2.5 mm/a. The sea level survey and assessment results showed that the sea level along the coast of Guangxi has been at a historically high level since 2001. The mean sea level from 2001 to 2010 was about 48 mm higher than the mean sea level from 1981 to 1990 and 22 mm higher than the mean from 1991 to 2000. While the mean sea level from 2011 to 2019 was about 46 mm higher than the mean from 2001 to 2010. In 2022, the sea level along the coast of Guangxi was 62 mm higher than normal, and it is expected that the sea level along the coast of Guangxi will rise another 45–135 mm over the next 30 years. From 1987 to 2021, the area of tidal flats in Guangxi decreased from 866.8 to 568.8 km^2, with a total decrease of 298 km^2. The decrease in the area of tidal flats and the increase in sea level showed a significant negative correlation.

2) Mangroves: Mangroves can reduce the rate of seawater deposition, facilitate sediment deposition, and accelerate the development of tidal flats, which, in turn, can provide more space for mangrove expansion [50], [51]. The coastal zone around Beibu Gulf has many mangroves, one of the world's highest concentrations of mangrove forests. This study showed that the area of mangrove forests in Beibu Gulf showed a stable upward trend from 1980 to 2020 [42], [52]. The rapid growth and seagoing expansion of mangroves have continuously covered tidal flat patches, resulting in a continuous reduction in tidal flat areas and an obvious negative correlation between tidal flats and mangroves [31]. In the case of the Shankou Mangrove National Nature Reserve, the largest in the coastal section of Guangxi, the mangrove area increased from 730 ha in 1990 to 919.6 ha in 2021 [42].

In contrast, the tidal flats in the area showed a continuous decreasing trend. Mangrove and tidal flats' center of mass shifted as shown in Fig. 14; both mangrove and tidal flats' center of mass shifted seaward as a whole, with the distance shifted being 0.7 km. The spatial distribution of mangroves showed a trend of seagoing expansion, and although the area of tidal flats was continuously reduced by mangrove expansion, its front was still continuously silted. The silt-promoting and sand sedimentation effects of mangrove forests may influence their continuous seaward siltation.

3) Impact of Riverine Sediment Loads Into the Sea: The amount of sediment flowing from rivers into seawater plays an important role in developing coastal tidal flats and forming tidal flat geomorphology [12]. There are many rivers in Beibu Gulf, such as the Nanliu, Beilun, Qinjiang, Fangcheng, Maoling, Red, and Majjiang rivers, which enter the sea, have rich sources of sedimentary materials, and play a significant role in shaping the surface of the estuary. The sediment continued to be pushed offshore from the estuary, increasing the number of tidal flats [39], [46]. According to relevant statistics, in recent decades, affected by the construction of reservoirs, industrial and agricultural water use, and a series of human activities, the amount of sand transported by rivers in Beibu Gulf has shown an obvious downward trend [11], [53], [54], [55], [56]. For example, the suspended sediment content in the Nanliu River Basin decreased from an annual average of 0.16 kg/m^3 in 1972–2006 to an annual average of 0.11 kg/m^3 in 2007–2020 [57]. According to water and sediment data from the Qinjiang Luwu Hydrology Station, since 1971, the average annual discharge and sediment transport of the Qinjiang River have shown a trend of fluctuation

[3][Online]. Available: https://www.mnr.gov.cn/sj/sjfw/hy/gbgg/zghpmgb/

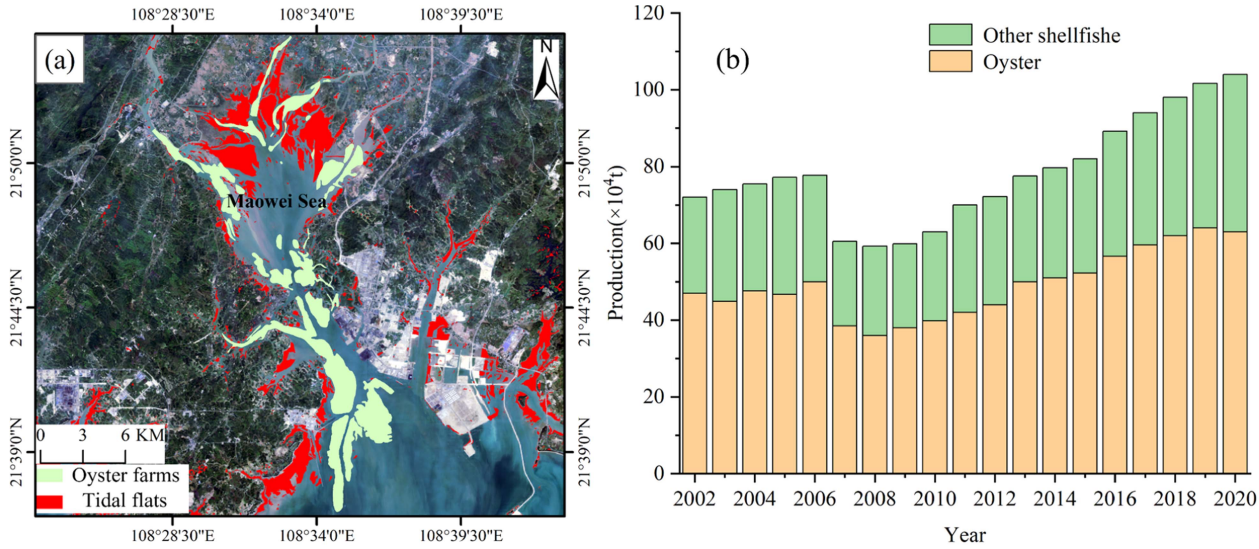

Fig. 15. Changes of oyster aquaculture production in Guangxi from 2002 to 2020. (a) Oyster farms and tidal flats in the Maowei Sea area in 2020. (b) Changes in oyster production in the coastal section of Guangxi, China.

and decline. From 1957 to 2016, the annual average sediment transport showed a continuous trend of fluctuation and decline, and the decline rate was approximately 0.67×104t/a [55], [56]. The reduction in incoming sediment has led to erosion retreat or siltation slowdown in estuarine tidal flats, which, to some extent, has caused a reduction in the tidal flat area in Beibu Gulf.

In addition, tidal currents can have a dynamic effect on sedimentary material on the beach surface, causing cyclical changes in the tidal flat elevation [38], [58]. The dual dynamic action of tides and wind waves washes away the loose material on the surface, causing shallow subsidence and lowering beach height. Taking the east coast of the Maowei Sea as an example, the water current was relatively turbulent, especially at 72 Jing, located next to the natural tidal waterway of Longmen, where seawater rushes rapidly. Its tidal velocity can reach a maximum value of 1.8 m/s, and the tidal flats in the vicinity were vulnerable to the impact of seawater erosion [59]. Seasonal changes in tides periodically affect the sediment on the beach surface. Spring tides reduce the sediment of the tidal flats, and winter tides promote the sediment of the tidal flats.

4) Impacts of Inshore Mariculture: Extensive oyster aquaculture can result in reduced hydrodynamics, prolong the water circulation cycle, and contribute to the deposition of suspended sediments, which in turn causes the siltation of mudflats [60]. The amount of oyster aquaculture in the offshore waters of Beibu Gulf is concentrated and huge, and the production of oyster aquaculture in the coastal section of Guangxi increased from 200 000 tons in 2002 to 400 000 tons in 2020 (see Fig. 15) [61], [62]. For example, the Maowei Sea is China's largest natural oyster spawning and breeding area [63], [64]. According to relevant studies, the amount of oyster farming in the region increased five-fold between 2011 and 2019 [48]. Many oyster piles and rows were randomly placed in the sea, which seriously affected the marine ecological environment, resulting in different degrees of siltation, seabed elevation, and poor drainage in the areas where the seedlings were collected [65]. The analyses revealed that the tidal flat area on the west coast of Kwangsi showed a slow increasing trend from 2012 to 2019, positively correlated with an increasing trend in oyster aquaculture volume. Therefore, in addition to the siltation effect of tidal flats caused by natural factors, large-scale oyster farming has also promoted the continuous growth of tidal flats.

5) Impact of Economic Development in Beibu Gulf: With the rapid economic development and population surge in Beibu Gulf, reclamation projects, port construction, and coastal zone development inevitably led to coastline expansion, coastal vegetation degradation, and reduced tidal flat areas [65], [66]. The population of Vietnam from 1987 to 2021 showed a rapid upward trend, from only 62.36 million in 1987 to 97.47 million in 2021, with a growth rate of 55.5% (see Fig. 16) (World Development Indicators). In 1982, the population of Hainan Province was 5 667 700, and by 2020, the population will reach 10 081 200, with a very rapid growth trend. The population of cities along the coast of China also showed a clear growth trend.[4]

In this study, a regression model was developed based on changes in tidal flats area and population, economy, and cargo throughput. After calculation, it was found that the correlation coefficients R of the change of tidal flat area with population, economy and cargo throughput were -0.74, -0.76, and -0.75, respectively, indicating that the decrease of the tidal flat area was significantly affected by the factors of population, economy and cargo throughput in the coastal area.

The influence of economic construction factors on tidal flats is mainly reflected in the construction of reclamation projects, port terminals, and the development of the coastal aquaculture industry and capital [67]. Coastal engineering construction is prone to change river water runoff and sediment transport and deposition processes, reducing sediment transport into the sea,

[4][Online]. Available: https://www.resdc.cn/

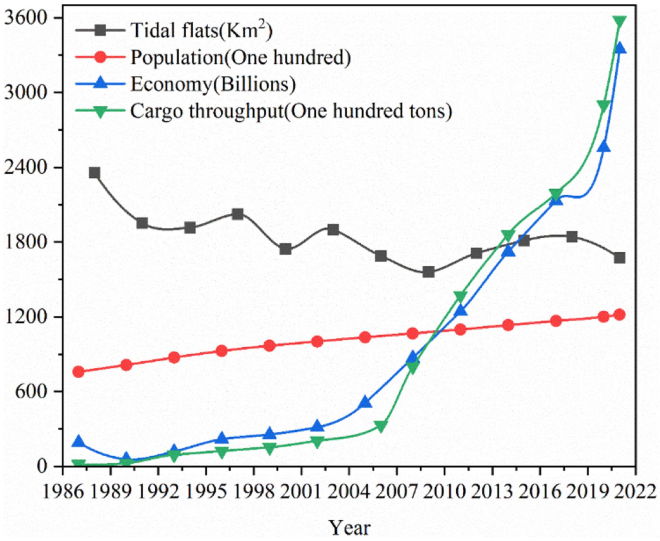

Fig. 16. Temporal changes of tidal flats, population, economy, cargo throughput in Beibu Gulf from 1987 to 2021.

thus affecting the hydrological conditions and sediment supply in the tidal flat area and ultimately affecting the change in tidal flat areas [68], [69]. Vietnam's coastline grew by 157 km between 1990 and 2010, significantly increasing the artificial coastline. With the deepening of open cooperation between China and ASEAN and the implementation of China's "One Belt, One Road" and other strategies, economic development has shown a trend towards the sea, and the tidal flats have been damaged to a greater extent by the new construction and expansion of various types of coastal projects [70], [71].

Based on the analysis of the characteristics of tidal flat area change and spatiotemporal fragmentation in the study area, it can be seen that the coastal population and economic growth are negatively correlated with changes in tidal flats. Under the joint action of rapid population growth and economic development, the tidal flats along Beibu Gulf are currently facing great resource pressure. The conflict between coastal areas' social and economic development and protecting coastal tidal flat resources has become increasingly serious.

VI. Conclusion

This article used the coastal zone around Beibu Gulf as the study area and comprehensively utilized Landsat series images, DEM data, and sea-level change data to build a fast, stable, and accurate tidal flat extraction algorithm to achieve large-scale and high-precision tidal flat extraction in Beibu Gulf. The spatiotemporal characteristics of the tidal flats in Beibu Gulf and the main driving factors were analyzed. The main conclusions are as follows.

1) An automatic tidal flat extraction algorithm was constructed to extract the spatiotemporal distribution of tidal flats in the Beibu Gulf from 1987 to 2021. The overall accuracy of the tidal flat extraction method used in this study reached 93.9%, the kappa coefficient reached 0.82, and the user and mapping accuracies of the tidal flats were greater than 85%. The results of qualitative and quantitative analyses showed that the tidal flat extraction method is feasible and accurate.
2) The total tidal flats area of the Beibu Gulf decreased from 2355.6 to 1671.7 km^2 in 35 years, a decrease of 29%, with an annual rate of change of −19.5 km^2/a. The tidal flats exhibited a stepwise downward trend from 1987 to 2000. The rate of decrease in the tidal flat inventory slowed and then increased from 2003 to 2018 and is likely to continue to show a downward trend. Among the three coastal segments, the tidal flats from Guangxi to Guangdong decreased the most, with a decrease of 34.4% over 35 years.
3) The fragmentation of tidal flats in Beibu Gulf increased over time, and the tidal flat patch density from Guangxi to Guangdong in China increased from 21.25 in 1987 to 34.53 in 2021. The natural drivers of changes in the spatiotemporal evolution of tidal flats and increased fragmentation were mainly sea-level rise, reduction in the sediment load of rivers entering the sea, and expansion of mangroves, among which sea-level rise had a significant impact on the reduction of tidal flat areas. Human-driven forces were mainly coastal economic development and offshore aquaculture.

References

[1] N. J. Murray et al., "High-resolution mapping of losses and gains of Earth's tidal wetlands," *Science*, vol. 376, no. 6594, pp. 744–749, 2022, doi: 10.1126/science.abm9583.
[2] X. Wang et al., "Tracking annual changes of coastal tidal flats in China during 1986–2016 through analyses of Landsat images with Google Earth Engine," *Remote Sens. Environ.*, vol. 238, 2020, Art. no. 110987, doi: 10.1016/j.rse.2018.11.030.
[3] S. Ghosh, D. R. Mishra, and A. A. Gitelson, "Long-term monitoring of biophysical characteristics of tidal wetlands in the northern Gulf of Mexico — A methodological approach using MODIS," *Remote Sens. Environ.*, vol. 173, pp. 39–58, 2016, doi: 10.1016/j.rse.2015.11.015.
[4] X. Wang et al., "Rebound in China's coastal wetlands following conservation and restoration," *Nature Sustainability*, vol. 4, no. 12, pp. 1076–1083, 2021, doi: 10.1038/s41893-021-00793-5.
[5] E. B. Barbier, "A global strategy for protecting vulnerable coastal populations," *Science*, vol. 345, no. 6202, pp. 1250–1251, 2014, doi: 10.1126/science.1254629.
[6] M. E. Hauer et al., "Sea-level rise and human migration," *Nature Rev. Earth Environ.*, vol. 1, no. 1, pp. 28–39, 2020, doi: 10.1038/s43017-019-0002-9.
[7] P. A. Sandifer and G. I. Scott, "Coastlines, coastal cities, and climate change: A perspective on urgent research needs in the United States," *Front. Mar. Sci.*, vol. 8, 2021, Art. no. 631986, doi: 10.3389/fmars.2021.631986.
[8] D. Sengupta, R. Chen, and M. E. Meadows, "Building beyond land: An overview of coastal land reclamation in 16 global megacities," *Appl. Geogr.*, vol. 90, pp. 229–238, 2018, doi: 10.1016/j.apgeog.2017.12.015.
[9] S. Temmerman, P. Meire, T. J. Bouma, P. M. Herman, T. Ysebaert, and H. J. De Vriend, "Ecosystem-based coastal defence in the face of global change," *Nature*, vol. 504, no. 7478, pp. 79–83, 2013, doi: 10.1038/nature12859.
[10] S. Brown et al., "Sea-level rise impacts and responses: A global perspective," in *Coastal Hazards*. New York, NY, USA: Springer, 2013, pp. 117–149, doi: 10.1007/978-94-007-5234-4_5.
[11] S. Dai, S. Yang, and M. Li, "The sharp decrease in suspended sediment supply from China's rivers to the sea: Anthropogenic and natural causes," *Hydrological Sci. J.*, vol. 54, no. 1, pp. 135–146, 2009, doi: 10.1623/hysj.54.1.135.
[12] Z. Dai, S. Fagherazzi, X. Mei, and J. Gao, "Decline in suspended sediment concentration delivered by the Changjiang (Yangtze) River into the East China Sea between 1956 and 2013," *Geomorphology*, vol. 268, pp. 123–132, 2016, doi: 10.1016/j.geomorph.2016.06.009.
[13] Z. Ma et al., "Rethinking China's new great wall," *Science*, vol. 346, no. 6212, pp. 912–914, 2014, doi: 10.1126/science.1257258.

[14] S. L. Yang, K. H. Xu, J. D. Milliman, H. F. Yang, and C. S. Wu, "Decline of Yangtze River water and sediment discharge: Impact from natural and anthropogenic changes," *Sci. Rep.*, vol. 5, no. 1, 2015, Art. no. 12581, doi: 10.1038/srep12581.

[15] N. J. Murray et al., "The global distribution and trajectory of tidal flats," *Nature*, vol. 565, no. 7738, pp. 222–225, 2019, doi: 10.1038/s41586-018-0805-8.

[16] S. Yang and H. Xu, "Tidal flat sediments and sedimentation on the Changxin and Hengsa Islands at the mouth of Changjiang River (in Chinese)," *Oceanographic Literature Rev.*, vol. 6, no. 42, pp. 450–451, 1995, doi: 10.11821/xb199405007.

[17] J. Choi, J. Ryu, Y. Lee, H. Yoo, H. J. Woo, and C. H. Kim, "Quantitative estimation of intertidal sediment characteristics using remote sensing and GIS," *Estuarine, Coastal Shelf Sci.*, vol. 88, no. 1, pp. 125–134, 2010, doi: 10.1016/j.ecss.2010.03.019.

[18] B. Fu et al., "Collaborative multiple change detection methods for monitoring the spatio-temporal dynamics of mangroves in Beibu Gulf, China," *GISci. Remote Sens.*, vol. 60, no. 1, 2023, Art. no. 2202506, doi: 10.1080/15481603.2023.2202506.

[19] W. Sun et al., "Coastline extraction using remote sensing: A review," *GISci. Remote Sens.*, vol. 60, no. 1, 2023, Art. no. 2243671, doi: 10.1080/15481603.2023.2243671.

[20] A. Campbell and Y. Wang, "Examining the influence of tidal stage on salt marsh mapping using high-spatial-resolution satellite remote sensing and topobathymetric LiDAR," *IEEE Trans. Geosci. Remote Sens.*, vol. 56, no. 9, pp. 5169–5176, Sep. 2018, doi: 10.1109/TGRS.2018.2810503.

[21] G. Zhou, C. Li, D. Zhang, D. Liu, X. Zhou, and J. Zhan, "Overview of underwater transmission characteristics of oceanic LiDAR," *IEEE J. Sel. Topics Appl. Earth Observ. Remote Sens.*, vol. 14, pp. 8144–8159, Jul. 27, 2021, doi: 10.1109/JSTARS.2021.3100395.

[22] G. Zhou and X. Zhou, "Seamless fusion of LiDAR and aerial imagery for building extraction," *IEEE Trans. Geosci. Remote Sens.*, vol. 52, no. 11, pp. 7393–7407, Nov. 2014, doi: 10.1109/TGRS.2014.2311991.

[23] Z. Xue and S. Qian, "Generalized composite mangrove index for mapping mangroves using Sentinel-2 Time series data," *IEEE J. Sel. Topics Appl. Earth Observ. Remote Sens.*, vol. 15, pp. 5131–5146, 2022, doi: 10.1109/JSTARS.2022.3185078.

[24] Z. Xue and S. Qian, "Two-Stream translating LSTM network for mangroves mapping using Sentinel-2 Multivariate time series," *IEEE Trans. Geosci. Remote Sens.*, vol. 61, Feb. 27, 2023, Art. no. 4401416, doi: 10.1109/TGRS.2023.3249179.

[25] M. Jia, Z. Wang, D. Mao, C. Ren, C. Wang, and Y. Wang, "Rapid, robust, and automated mapping of tidal flats in China using time series Sentinel-2 images and Google Earth Engine," *Remote Sens. Environ.*, vol. 255, 2021, Art. no. 112285, doi: 10.1016/j.rse.2021.112285.

[26] M. A. Friedl et al., "MODIS Collection 5 global land cover: Algorithm refinements and characterization of new datasets," *Remote Sens. Environ.*, vol. 114, no. 1, pp. 168–182, 2010, doi: 10.1016/j.rse.2009.08.016.

[27] M. B. Lyons, S. R. Phinn, and C. M. Roelfsema, "Long term land cover and seagrass mapping using Landsat and object-based image analysis from 1972 to 2010 in the coastal environment of South East Queensland, Australia," *ISPRS J. Photogramm. Remote Sens.*, vol. 71, pp. 34–46, 2012, doi: 10.1016/j.isprsjprs.2012.05.002.

[28] N. Kiggundu, L. Abugri Anaba, N. Banadda, J. Wanyama, and I. Kabenge, "Assessing land use and land cover changes in the Murchison Bay catchment of Lake Victoria basin in Uganda," *J. Sustain. Develop.*, vol. 11, no. 1, 2018, Art. no. 44, doi: 10.5539/jsd.v11n1p44.

[29] N. J. Murray, S. R. Phinn, R. S. Clemens, C. M. Roelfsema, and R. A. Fuller, "Continental scale mapping of tidal flats across East Asia using the Landsat archive," *Remote Sens.*, vol. 4, no. 11, pp. 3417–3426, 2012, doi: 10.3390/rs4113417.

[30] N. J. Murray, R. S. Clemens, S. R. Phinn, H. P. Possingham, and R. A. Fuller, "Tracking the rapid loss of tidal wetlands in the Yellow Sea," *Front. Ecol. Environ.*, vol. 12, no. 5, pp. 267–272, 2014, doi: 10.1890/130260.

[31] E. Gao and G. Zhou, "Spatio-Temporal changes of Mangrove-Covered tidal flats over 35 years using satellite remote sensing imageries: A case study of Beibu Gulf, China," *Remote Sens.*, vol. 15, no. 7, 2023, Art. no. 1928, doi: 10.3390/rs15071928.

[32] S. Sagar, D. Roberts, B. Bala, and L. Lymburner, "Extracting the intertidal extent and topography of the Australian coastline from a 28 year time series of Landsat observations," *Remote Sens. Environ.*, vol. 195, pp. 153–169, 2017, doi: 10.1016/j.rse.2017.04.009.

[33] S. Dai et al., "Constructing of tidal flat extraction index in coastal zones using Sentinel-2 multispectral images," *Spectrosc. Spectral Anal.*, vol. 43, no. 06, pp. 1888–1894, 2023. [Online]. Available: https://www.gpxygpfx.com/EN/Y2023/V43/I06/1888

[34] Y. Hu et al., "Mapping coastal salt marshes in China using time series of Sentinel-1 SAR," *ISPRS-J. Photogramm. Remote Sens.*, vol. 173, pp. 122–134, 2021, doi: 10.1016/j.isprsjprs.2021.01.003.

[35] J. Liang, C. Chen, W. Sun, G. Yang, Z. Liu, and Z. Zhang, "Spatio-temporal land use/cover change dynamics in Hangzhou Bay, China, using long-term Landsat time series and GEE platform," *J. Remote Sens.*, vol. 27, no. 6, pp. 1480–1495, 2023, doi: 10.11834/jrs.20232614.

[36] W. Yang et al., "Monitoring tidal flats boundaries through combining Sentinel-1 and Sentinel-2 imagery," *Environ. Technol. Innov.*, vol. 22, 2021, Art. no. 101401, doi: 10.1016/j.eti.2021.101401.

[37] N. Otsu, "A threshold selection method from gray-level histograms," *IEEE Trans. Syst., Man, Cybern.*, vol. 9, no. 1, pp. 62–66, Jan. 1979, doi: 10.1109/TSMC.1979.4310076.

[38] G. Zhou, J. Huang, T. Yue, Q. Luo, and G. Zhang, "Temporal-spatial distribution of wave energy: A case study of Beibu Gulf, China," *Renewable Energy*, vol. 74, pp. 344–356, 2015, doi: 10.1016/j.renene.2014.08.014.

[39] R. Tang, Z. Dai, X. Zhou, and S. Li, "Tropical cyclone-induced water and suspended sediment discharge delivered by mountainous rivers into the Beibu Gulf, South China," *Geomorphology*, vol. 389, 2021, Art. no. 107844, doi: 10.1016/j.geomorph.2021.107844.

[40] B. Gao, "NDWI—A normalized difference water index for remote sensing of vegetation liquid water from space," *Remote Sens. Environ.*, vol. 58, no. 3, pp. 257–266, 1996, doi: 10.1016/S0034-4257(96)00067-3.

[41] H. Xu, "Modification of normalised difference water index (NDWI) to enhance open water features in remotely sensed imagery," *Int. J. Remote Sens.*, vol. 27, no. 14, pp. 3025–3033, 2006, doi: 10.1080/01431160600589179.

[42] M. Jia, Z. Wang, D. Mao, C. Huang, and C. Lu, "Spatial-Temporal changes of China's Mangrove forests over the past 50 years: An analysis towards the sustainable development goals (SDGs)," *Chin. Sci. Bull*, vol. 66, no. 30, pp. 3886–3901, 2021, doi: 10.1360/TB-2020-1412.

[43] M. Jia et al., "Mapping global distribution of Mangrove forests at 10-m resolution," *Sci. Bull.*, vol. 68, no. 12, pp. 1306–1316, 2023, doi: 10.1016/j.scib.2023.05.004.

[44] Y. Li and Z. Niu, "Systematic method for mapping fine-resolution water cover types in China based on time series Sentinel-1 and 2 images," *Int. J. Appl. Earth Observation Geoinf.*, vol. 106, 2022, Art. no. 102656, doi: 10.1016/j.jag.2021.102656.

[45] B. S. Chen, T. Tsay, K. Chiang, and C. Yang, "Regional connectivity in modified finite point method," *Eng. Anal. Boundary Elements*, vol. 47, pp. 21–31, 2014, doi: 10.1016/j.enganabound.2014.05.001.

[46] D. Li, J. Li, and W. Tuan, "Tidal analysis of Long-Term observation data of tide gauges along Vietnam coast," *Hydrographic Surveying Charting*, vol. 37, no. 3, pp. 29–52, 2017, doi: 10.3969/j.issn.1671-3044.2017.03.006.

[47] C. Tong et al., "The effects of landscape pattern change on ecosystem services value in the coastal zone of the East China Sea," *J. ZheJiang Univ. (Sci. Ed.)*, vol. 47, no. 4, pp. 492–507, 2020, doi: 10.3785/j.issn.1008-9497.2020.04.013.

[48] X. Liang, R. Wang, Z. Dai, J. Wang, H. Huang, and S. Li, "Spatial-temporal variations of bare flats in the Qinjiang River estuary, Maowei Sea," *Mar. Geol. Quaternary Geol.*, vol. 43, no. 3, pp. 107–118, 2023, doi: 10.16562/j.cnki.0256-1492.2022091201.

[49] Q. Han, Z. Niu, M. Wu, and J. Wang, "Remote-sensing monitoring and analysis of China intertidal zone changes based on tidal correction," *Chin. Sci. Bull.*, vol. 64, no. 4, pp. 456–473, 2018, doi: 10.1360/N972018-00723.

[50] Y. Chen, Y. Li, C. Thompson, X. Wang, T. Cai, and Y. Chang, "Differential sediment trapping abilities of Mangrove and Saltmarsh vegetation in a subtropical estuary," *Geomorphology*, vol. 318, pp. 270–282, 2018, doi: 10.1016/j.geomorph.2018.06.018.

[51] A. Swales, S. J. Bentley Sr, and C. E. Lovelock, "Mangrove-forest evolution in a sediment-rich estuarine system: Opportunists or agents of geomorphic change?," *Earth Surf. Processes Landforms*, vol. 40, no. 12, pp. 1672–1687, 2015, doi: 10.1002/esp.3759.

[52] Y. Chang, J. Liao, and L. Zhang, "Temporal and spatial variations of mangroves and their driving factors in Southeast Asia," *Trop. Geogr.*, vol. 43, no. 1, pp. 31–42, 2023, doi: 10.13284/j.cnki.rddl.003610.

[53] T. H. Dang, A. Coynel, D. Orange, G. Blanc, H. Etcheber, and L. A. Le, "Long-term monitoring (1960–2008) of the river-sediment transport in the Red River Watershed (Vietnam): Temporal variability and dam-reservoir impact," *Sci. Total Environ.*, vol. 408, no. 20, pp. 4654–4664, 2010, doi: 10.1016/j.scitotenv.2010.07.007.

[54] J. Gao et al., "Interference of natural and anthropogenic forcings on variations in continental freshwater discharge from the Red River (Vietnam) to sea," *Quaternary Int.*, vol. 380, pp. 133–142, 2015, doi: 10.1016/j.quaint.2015.01.007.

[55] S. Li and H. Huang, "Variations of runoff and sediment in Qinjiang River in the past 50 years," *Guangxi Sci.*, vol. 25, no. 4, pp. 409–417, 2018, doi: 10.13656/j.cnki.gxkx.20180801.002.
[56] J. Mo, Y. Lu, D. Wang, and P. Huang, "Analysis of interannual water-sediment variation law of Qinjiang River Basin in Guangxi," *Water Resour. Hydropower Eng.*, vol. 51, no. 1, pp. 130–138, 2020, doi: 10.13928/j.cnki.wrahe.2020.01.015.
[57] S. Li, X. Yang, H. Huang, X. Liang, R. Wang, and B. Feng, "Variations in the suspended sediment concentration in mountain-type rivers flowing into the sea in the past 60 years—Taking Nanliu River in Beibu Gulf as an example," *Front. Earth Sci.*, vol. 10, 2022, Art. no. 913022, doi: 10.3389/feart.2022.913022.
[58] S. Moskalski and R. Torres, "Influences of tides, weather, and discharge on suspended sediment concentration," *Continental Shelf Res.*, vol. 37, pp. 36–45, 2012, doi: 10.1016/j.csr.2012.01.015.
[59] C. Wang, L. Cai, Y. Wu, and Y. Ouyang, "Numerical simulation of the impact of an integrated renovation project on the Maowei Sea hydrodynamic environment," *Sci. Rep.*, vol. 11, no. 1, 2021, Art. no. 17059, doi: 10.1038/s41598-021-96441-1.
[60] P. Gernez, D. Doxaran, and L. Barillé, "Shellfish aquaculture from space: Potential of Sentinel 2 to monitor tide-driven changes in turbidity, chlorophyll concentration and oyster physiological response at the scale of an oyster farm," *Front. Mar. Sci.*, vol. 4, 2017, Art. no. 137, doi: 10.3389/fmars.2017.00137.
[61] G. S. Bureau, *Guangxi Statistical Yearbook*. Beijing, China: China Statistics Press, 2017, pp. 366–369.
[62] Y. Pan, J. Li, W. Huang, and Y. Ren, "Analysis of current situations, existing problems of oyster industry and its developmental suggestions in Guangxi," *J. South. Agric*, vol. 52, no. 9, pp. 2608–2618, 2021, doi: 10.3969/j.issn.2095-1191.2021.09.032.
[63] Y. Gu, H. Huang, Y. Liu, X. Gong, and X. Liao, "Non-metric multidimensional scaling and human risks of heavy metal concentrations in wild marine organisms from the Maowei Sea, the Beibu Gulf, South China Sea," *Environ. Toxicol. Pharmacol.*, vol. 59, pp. 119–124, 2018, doi: 10.1016/j.etap.2018.03.002.
[64] C. Xu et al., "Spatiotemporal variations of biogenic elements and sources of sedimentary organic matter in the largest oyster mariculture bay (Maowei Sea), Southwest China," *Sci. Total Environ.*, vol. 730, 2020, Art. no. 139056, doi: 10.1016/j.scitotenv.2020.139056.
[65] L. Yang, L. Yang, and H. Pan, "Characteristics of recent evolution in Qinzhou Bay influenced by human activities," *J. Trop. Oceanogr.*, vol. 38, no. 6, pp. 41–50, 2019. [Online]. Available: http://www.jto.ac.cn/EN/10.11978/2019013
[66] D. Zhao, M. Xiao, C. Huang, Y. Liang, and Z. Yang, "Land use scenario simulation and ecosystem service management for different regional development models of the Beibu Gulf Area, China," *Remote Sens.*, vol. 13, no. 16, 2021, Art. no. 3161, doi: 10.3390/rs13163161.
[67] X. Bi, F. Liu, and X. Pan, "Coastal projects in China: From reclamation to restoration," *Environ. Sci. Technol.*, vol. 46, no. 9, pp. 4691–4692, 2012, doi: 10.1021/es301286d.
[68] C. Xu and W. Liu, "The spatiotemporal assessments for tidal flat erosion associated with urban expansion in the conterminous coastal United States from 1985 to 2015," *Sci. Total Environ.*, vol. 899, 2023, Art. no. 165660, doi: 10.1016/j.scitotenv.2023.165660.
[69] M. Zhang et al., "Tidal-flat reclamation aggravates potential risk from storm impacts," *Coast. Eng.*, vol. 166, 2021, Art. no. 103868, doi: 10.1016/j.coastaleng.2021.103868.
[70] Y. Li, L. Sun, Z. Wu, and H. Liu, "Evaluation and obstacle factors of marine resources and environment carrying capacity in Beibu Gulf Urban Agglomeration," *Front. Mar. Sci.*, vol. 10, 2023, Art. no. 1196196, doi: 10.3389/fmars.2023.1196196.
[71] M. Ou, X. Lai, and J. Gong, "Territorial pattern evolution and its comprehensive carrying capacity evaluation in the coastal area of Beibu Gulf, China," *Int. J. Environ. Res. Public Health*, vol. 19, no. 17, 2022, Art. no. 10469, doi: 10.3390/ijerph191710469.

Ertao Gao received the M.S. degree in photogrammetry and remote sensing engineering from South West Jiaotong University, Chengdu, China, in 2017. He is currently working toward the Ph.D. degree in remote sensing major with the Guilin University of Technology, Guilin, China.

Since 2017, he has been a Teacher with the College of Geomatics and Geoinformation, Guilin University of Technology. His research interests include remote sensing of coastal wetland and bathymetry inversion of remote sensing.

Guoqing Zhou (Senior Member, IEEE) received the Ph.D. degree in photogrammetry and remote sensing from Wuhan University, Wuhan, China, in 1994.

He was a Researcher with the Department of Computer Science and Technology, Tsinghua University, Beijing, China, and a Postdoctoral Researcher with the Institute of Information Science, Beijing Jiaotong University, Beijing. He continued his research as an Alexander von Humboldt Fellow with the Technical University of Berlin, Berlin, Germany, from 1996 to 1998, and was a Postdoctoral Researcher with The Ohio State University, Columbus, OH, USA, from 1998 to 2000. He was an Assistant Professor, an Associate Professor, and a Full Professor with Old Dominion University, Norfolk, VA, USA, in 2000, 2005, and 2010, respectively. He has authored 10 books, 7 book chapters, and published 578 peer-refereed papers with more than 296 articles in prestigious journals.

Shuxian Li (Student Member, IEEE) received the Bachelor of Engineering degree in remote sensing science and technology in 2023 from the Guilin University of Technology, Guilin, China, where she is currently working toward the M.S. degree in remote sensing.

Her research interests include remote sensing techniques and applications, especially coastal zone remote sensing.

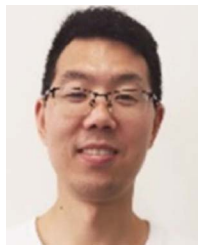

Bolin Fu received the B.S. degree in geographical science from Hubei Normal University, Huangshi, China, in 2012, and the Ph.D. degree in cartography and geographic information system from the Northeast Institute of Geography and Agroecology, Chinese Academy of Sciences, Changchun, China, in 2017.

He is currently an Associate Professor with the College of Geomatics and Geoinformation, Guilin University of Technology, Guilin, China. His research interests include active and passive remote sensing.

Yunzhi Xiao received the Bachelor of Engineering degree in remote sensing science and technology from the Guilin University of Technology, Guilin, China, in 2023.

His research interests mainly include the monitoring and analysis of long-term changes in tidal flats.

Yanping Lan received the Bachelor of Engineering degree in remote sensing science and technology in 2021 from the Guilin University of Technology, Guilin, China, where she is currently working toward the M.S. degree in remote sensing.

Her research interests include remote sensing techniques and applications, especially ecological remote sensing and landscape ecology research.

Feng Wang received the Ph.D. degree in photogrammetry and remote sensing from the Faculty of Geosciences and Environmental Engineering, Southwest Jiaotong University, Chengdu, China in 2020.

He is an Associate Professor with the College of Geomatics and Geoinformation, Guilin University of Technology, Guilin, China. His research interests include photogrammetry, point clouds processing, and 3-D modeling.

Jiasheng Xu received the B.S. degree in electronic business management and M.S. degree in remote sensing engineering in 2013 and 2017, respectively, from the Guilin University of Technology, Guilin, China, where he is currently working toward the Ph.D. degree in remote sensing.

From 2015 to 2017, he was a Teacher with computer application Department, Guilin University of Technology. His research interests include exploration, ocean, bathymetry, and water quality inversion of remote sensing.

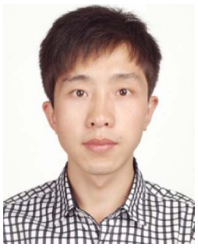

Qiang Zhu received the M.S. degree in remote sensing engineering from the College of Tourism, Guilin University of Technology, Guilin, China, in 2019. He is currently working toward the Ph.D. degree in remote sensing major with the Guilin University of Technology.

His research interests geomatics and spatial information technology.

Yuhang Bai, was born in August 1993 in Huinan, Jilin Province, China. He received the master's degree in geology from Guilin University of Technology, Guilin, China, in 2019. He is currently working toward the Ph.D. degree in remote sensing major with the Guilin University of Technology, Guilin, China.

His research interests include Geological Resources and Geological Engineering.